

ANALYTICAL SOLUTIONS OF DOWNSLOPE MOTIONS

Sang Jianguo (桑建国)

Department of Geophysics, Peking University, Beijing

Received October 12, 1989

ABSTRACT

The solutions of downslope motions over a sloping terrain are solved analytically in terms of the atmospheric wave equations with a two-layer model. The physical meanings of the solutions are discussed. As the lower layer of the atmosphere is stable and deep with strong wind the solution represents strong downslope wind, while as the lower layer is strong stable with light wind the drainage flow is obtained. The dependence of the strength of downslope motion on the atmospheric stratification, wind field structure as well as Scorer parameter is also examined.

Key words: downslope motion, atmospheric waves, leeside wind, drainage flow

I. INTRODUCTION

The downslope motion in the present paper means two kinds of atmospheric circulations. One is the phenomenon of strong wind and sudden warming in the leeside as the air flows over plateau, mountain or tableland. This kind of circulation often occurs as wind speed is strong and terrain is steep. The other phenomenon is the drainage flow, which forms as the cold air induced by the nocturnal radiative cooling coasts down along a slope. Since it is related with the surface radiative inversion the drainage often occurs at clear night with weak wind. Provided the radiative cooling is strong enough the drainage can form even over a slope with height of only one or two hundred meters.

Some analytical analyses have been made for the two kinds of downslope motions. Klemp and Lilly (1975), for example, used linearized three-layer model to discuss the upstream atmospheric conditions inducing the strong surface wind in the leeside slope. They argued that it favours the strong wind in the leeside if the atmosphere in the lower layer is stable and in the middle troposphere is deep and less stable.

For the drainage flow, Fleagle (1950) attributed the horizontal pressure gradient force to buoyant force produced by radiative cooling, and obtained the analytical solution of the drainage flow. In his solution, the horizontal velocity is directly proportional to the net radiation but inversely proportional to the depth of the cooling layer and the slope of the terrain. Since the formations of all the downslope motions need stable lower layer atmosphere, certain difference of values of Scorer parameters between higher and lower atmospheres, and corresponding sloping terrain, the two kinds of motions must have similar mathematical expressions even though they have different mechanisms of generation. In the present paper a two-layer model is used to solve the atmospheric wave equation analytically. In given atmospheric and topographic conditions the analytical solutions of the disturbed streamlines are obtained. For different values of the parameters the solution represents different forms of motions. The

solutions are discussed in the physical respect and compared with other theoretical and observational results.

II. SOLUTIONS OF THE ATMOSPHERIC WAVE EQUATION

A two-layer model with the interface at $z=0$ is considered. The depth of the lower layer of the model is set to be h . Then the ground surface is at $z=-h$. The Brunt-Vaisala frequencies and the mean wind speeds in the lower and higher layers are assumed as N_1 , N_2 , U_1 and U_2 , respectively. As air flows over the terrain at the bottom boundary of the model the vertical displacements of the disturbed streamlines are $\xi = z - z_0$, where z is the height of the disturbed streamlines and z_0 is the height of the undisturbed streamlines far upstream. According to the wave theory (Scorer, 1978) ξ satisfies the wave equation

$$\frac{\partial^2 \xi_i}{\partial x^2} + \frac{\partial^2 \xi_i}{\partial z^2} + l_i^2 \xi_i = 0, \quad (1)$$

where $i=1,2$ represent the lower and higher atmosphere, respectively, and $l_i = N_i/U_i$ is the Scorer parameter.

Expanding ξ as Fourier components in wavenumber space,

$$\xi = \tilde{\xi} e^{ikx}, \quad i = \sqrt{-1},$$

and substituting it into Eq. (1), we obtain the equation of the component $\tilde{\xi}$ with wavenumber k

$$\frac{\partial^2 \tilde{\xi}_i}{\partial z^2} - (k^2 - l_i^2) \tilde{\xi}_i = 0. \quad (2)$$

The downslope motions require the condition $N_1 > N_2$. Since usually $U_2 > U_1$, the condition $l_1 > l_2$ is always satisfied.

The solution of $\tilde{\xi}_1$ satisfying Eq. (2) is

$$\tilde{\xi}_1 = A \cos \nu_1 z + B \sin \nu_1 z, \quad (3)$$

where $\nu_1 = \sqrt{l_1^2 - k^2}$.

In the upper layer, $\tilde{\xi}_2$ consists of the waves with higher and lower wavenumbers, respectively. As $k < l_2$

$$\tilde{\xi}_2 = C e^{i\nu_2 z}, \quad (4)$$

where $\nu_2 = \sqrt{l_2^2 - k^2}$. Since the term including $e^{-i\nu_2 z}$ represents the waves propagating downward, it does not have physical meaning and must be omitted (Smith, 1979). As $k > l_2$,

$$\tilde{\xi}_2 = C e^{-\mu z}, \quad (5)$$

where $\mu = \sqrt{k^2 - l_2^2}$.

The coefficients A, B and C in the previous expressions will be determined according to the interface conditions and the bottom boundary condition.

The first interface condition is that the vertical displacements of the streamlines at both sides of the interface are continuous,

$$\xi_1 = \xi_2, \quad z = 0. \quad (6)$$

The second interface condition is determined according to the discontinuity of the density and the velocity, and the continuity of the pressure at the two sides of the interface. According to Bernoulli theorem along the streamline on the lower side of the interface, we have

$$\frac{p_0}{\rho_1} + \frac{1}{2}U_1^2 = \frac{p_1}{\rho_1} + \frac{1}{2}[(U_1 + u_1)^2 + w_1^2] + g\xi_1,$$

where the left-hand side represents the undisturbed state, while the right-hand side the disturbed state. u_1 and w_1 are the disturbed velocities. Expanding the right-hand side and omitting the second order quantities, we have

$$p_0 - p_1 = \rho_1 U_1 u_1 + \rho_1 g \xi_1.$$

Similarly, on the upper side of the interface, we have

$$p_0 - p_2 = \rho_2 U_2 u_2 + \rho_2 g \xi_2.$$

By using of $p_1 = p_2, u = -U \frac{\partial \xi}{\partial z}$, and the approximate relation $\frac{\rho_2}{\rho_1} \left(\frac{U_2}{U_1}\right)^2 \simeq \left(\frac{U_2}{U_1}\right)^2$,

we obtain the second interface condition,

$$\frac{\partial \xi_1}{\partial z} = \frac{g}{U_1^2} \frac{\rho_1 - \rho_2}{\rho_1} \xi_1 + \left(\frac{U_2}{U_1}\right)^2 \frac{\partial \xi_2}{\partial z}, \tag{7}$$

or

$$\frac{\partial \xi_1}{\partial z} = \gamma \xi_2 + \alpha \frac{\partial \xi_2}{\partial z}, \tag{8}$$

where parameters $\alpha = \left(\frac{U_2}{U_1}\right)^2$ and $\gamma = \frac{g}{U_1^2} \frac{\rho_1 - \rho_2}{\rho_1}$ represent the wind shear and density difference between upper and lower layers, respectively.

The topographic profile of the leeside slope is assumed as a arc tangent function

$$\xi_1 \Big|_{z=-h} = -a \arctan \left(\frac{x}{b} \right),$$

where a and b are the length scales of height and width of the terrain, respectively. The Fourier transformation of the expression above in wavenumber space is

$$\xi_1 \Big|_{z=-h} = -ai \int_0^\infty e^{-kb} / k e^{ibx} dk. \tag{9}$$

After Fourier transformation of Eqs. (6), (8) and (9), the interface and bottom boundary conditions, which ξ should satisfy, are expressed as

$$\xi_1 = \xi_2, \quad z=0 \tag{10}$$

$$\frac{\partial \xi}{\partial z} = \alpha \frac{\partial \xi_2}{\partial z} + \gamma \xi_2, \quad z=0 \tag{11}$$

$$\xi_1 = -aie^{-hb}/k. \quad z=-h \tag{12}$$

Using Eqs. (10)–(12) to determine the coefficients A , B and C , we obtain the solution of ξ as follows.

As $k < l_2$ the solution of ξ_1 is

$$\xi_{11} = -ia \frac{e^{-hb}}{k} P [(v_1 \cos v_1 h - \gamma \sin v_1 h) (v_1 \cos v_1 z + \gamma \sin v_1 z) - v_2^2 \alpha^2 \sin v_1 h \sin v_1 z + i v_1 v_2 a \sin v_1 (h + z)], \tag{13}$$

where $P = [(v_1 \cos v_1 h - \gamma \sin v_1 h)^2 + v_2^2 \alpha^2 \sin^2 v_1 h]^{-1}$.

As $k > l_2$ the solution is

$$\xi_{1h} = -ia \frac{e^{-kb}}{k} \frac{v_1 \cos v_1 z + (\gamma - a\mu) \sin v_1 z}{v_1 \cos v_1 h - (\gamma - a\mu) \sin v_1 h} \quad (14)$$

The disturbances of the streamlines consist of the higher wavenumber components ξ_{1h} and the lower wavenumber components ξ_{1l} ,

$$\xi_1 = \xi_{1l} + \xi_{1h} = \int_0^{l_2} \xi_{1l} e^{ikz} dk + \int_{l_2}^{\infty} \xi_{1h} e^{ikz} dk \quad (15)$$

In the first integral of Eq. (15) the integrand (see Eq. (13)) includes the factor of e^{-bz}/k which decreases rapidly with k . Then the main contribution of the integral consists of the lower wavenumber components (at the vicinity of $k=0$). Similar to the treatment by Scorer (1978), the integral can be represented as

$$\xi_{1l} = -aP^* [(l_1 \cos l_1 h - \gamma \sin l_1 h) (l_1 \cos l_1 z + \gamma \sin l_1 z) - l_2^2 \alpha^2 \sin l_1 h \sin l_1 z + il_1 l_2 \alpha \sin l_1 (h+z)] \int_0^{\infty} i \frac{e^{-kb}}{k} e^{ikz} dk \quad (16)$$

Taking the real part, we have

$$\xi_{1l} = -a \arctan \frac{x}{b} P^* [l_1 \cos l_1 h - \gamma \sin l_1 h] (l_1 \cos l_1 z + \gamma \sin l_1 z) - l_2^2 \alpha^2 \sin l_1 h \sin l_1 z, \quad (17)$$

where $P^* = P|_{k=0} = [(l_1 \cos l_1 h - \gamma \sin l_1 h)^2 + a^2 l_2^2 \sin^2 l_1 h]^{-1}$.

The second integral of Eq. (15) has a singularity at $k=k^*$ as the denominator of the integrand (see Eq. (14)) is zero,

$$v_1^* \cos v_1^* h - (\gamma - a\mu^*) \sin v_1^* h = 0, \quad (18)$$

where $v_1^* = \sqrt{l_1^2 - k^{*2}}$, $\mu^* = \sqrt{k^{*2} - l_2^2}$.

According to the residue theorem the integral can be calculated as

$$\xi_{1h} = \pi R i,$$

where the residue

$$R = -ia \frac{e^{-k^*b}}{k^*} \frac{[v_1^* \cos v_1^* z + (\gamma - a\mu^*) \sin v_1^* z] \cos v_1^* x}{\frac{\partial}{\partial k} [v_1 \cos v_1 h - \gamma \sin v_1 h + \mu \alpha \sin v_1 h]} \Big|_{k=k^*} \quad (19)$$

After rearranging we have

$$\xi_{1h} = \pi a \frac{e^{-k^*b}}{k^{*2}} \cdot \frac{v_1^{*3}}{\sin^2 v_1^* h} \cdot \frac{\sin v_1^* (h+z) \cos k^* x}{\mu^* \alpha - \gamma + v_1^{*2} h + \frac{v_1^{*2} \alpha}{\mu^*} + (\gamma - \mu^* \alpha)^2 h} \quad (20)$$

Substituting Eqs. (17) and (20) into Eq. (15), we obtain the solution of the disturbed streamlines in the lower layer. It can be seen from the numerical analyses in the following paragraph that the value of the higher wavenumber components is much less than that of the lower wavenumber components. Thus the flow disturbances induced by the topography consist mainly of the components with longer wavelengths. We will discuss this part of the solution in detail.

Substituting the relationship $w = U \partial \xi / \partial x$ into Eq. (17) obtains the lower wavenumber part of the disturbed vertical motion

$$w_{1l} = -U_1 \frac{ab}{b^2 + x^2} P^* [(l_1 \cos l_1 h - \gamma \sin l_1 h) (l_1 \cos l_1 z + \gamma \sin l_1 z) - l_2^2 \alpha^2 \sin l_1 h \sin l_1 z]. \quad (21)$$

Substituting Eq. (21) into $\partial(U_1 + u_1)/\partial x + \partial w_1/\partial z = 0$, integrating it with respect to x and using the condition of $u_1 = 0$ at $x = -\infty$, we have the lower wavenumber part of the disturbed horizontal velocity as

$$u_{1l} = U_1 a \left(\arctan \frac{x}{b} + \frac{\pi}{2} \right) P^* [(l_1 \cos l_1 h - \gamma \sin l_1 h) (-l_1^2 \sin l_1 z + \gamma l_1 \cos l_1 z) - l_2^2 l_1 \alpha^2 \sin l_1 h \cos l_1 z]. \quad (22)$$

The higher wavenumber part of the disturbed velocities can be deduced from Eq. (20). Since its value is small, the expression is omitted here.

Similar to the treatment of obtaining Eqs. (17), (20) etc., we can obtain the disturbed streamlines in the upper layer

$$\begin{aligned} \xi_2 = \xi_{2l} + \xi_{2h} = & -a \arctan \frac{x}{b} P^* [(l_1 \cos l_1 h - \gamma \sin l_1 h) l_1 \cos l_2 z - l_1 l_2 \alpha^2 \sin l_1 h \sin l_2 z] \\ & + \pi a \frac{e^{-k^* b}}{k^{*2}} \cdot \frac{v_1^* h}{\sin v_1^* h} \cdot \frac{e^{-\mu^* z} \cos k^* x}{\mu^* a - \gamma + v_1^{*2} h + \frac{v_1^{*2} \alpha}{\mu^*} + (\gamma - \mu^* a)^2 h}, \end{aligned} \quad (23)$$

and the expressions of u_{2l} , u_{2h} , w_{2l} and w_{2h} which are all omitted here.

III. DISCUSSION

1. Leaside Strong Wind

In the lower layer the atmosphere is assumed as follows: the depth $h = 3000$ m, $N_1 = 1.5 \times 10^{-2} \text{s}^{-1}$, the wind speed increases linearly with height and its mean value $U_1 = 15 \text{m/s}$, then the Scorer parameter $l_1 = 0.001 \text{m}^{-1}$. In the upper layer $N_2 = 1.25 \times 10^{-2} \text{s}^{-1}$, $U_2 = 25 \text{m/s}$, and then $l_2 = 0.0005 \text{m}^{-1}$. According to the distributions of the wind speeds and the potential temperature in the upper and the lower layers the condition of $\gamma = 0.001 \text{m}^{-1}$ can be suggested. Since it is assumed that the wind speed in the lower layer varies continuously with height, there is no shear in the vicinity of the interface, then $\alpha = 0$. The parameters of the terrain are assumed to be $a = 500$ m and $b = 2000$ m, that represent a sloping terrain with height of 1500 m and slope of 11° . The atmospheric conditions described above are similar to those given by Klemp and Lilly (1975) in their analytical solution of the strong downslope motion in a mountain leaside.

Substituting the parameters above into the expressions of ξ_{1l} and ξ_{2l} , we obtain the lower wavenumber part of the disturbed streamlines. The numerical calculation indicates that the maximum amplitude of the disturbances of lower wavenumbers is of the same order of the terrain height.

According to Eq. (19) it can be obtained with graphic method that $k^* = 0.000935$, $v_1^* = 0.000354$ and $\mu^* = 0.00079$. Substituting these parameters into Eqs. (20) and (23), we have the solution of higher wavenumber components. Their amplitudes are only about 20 m. Compared with the lower wavenumber components all the contributions by ξ_{1h} , ξ_{2h} as well as u_{1h} , u_{2h} , w_{1h} , w_{2h} can be omitted.

Fig. 1 shows the calculated wind vectors of V_1 and V_2 , where $V_1 = \sqrt{(U_1 + u_{1l})^2 + w_{1l}^2}$ and $V_2 = \sqrt{(U_2 + u_{2l})^2 + w_{2l}^2}$. From this figure it can be seen that the strong momentum at the higher levels over the upper end of the slope transports downward along the streamlines formed by the topographic waves. At the middle part of the slope (near $x = 0$), the vertical velocity

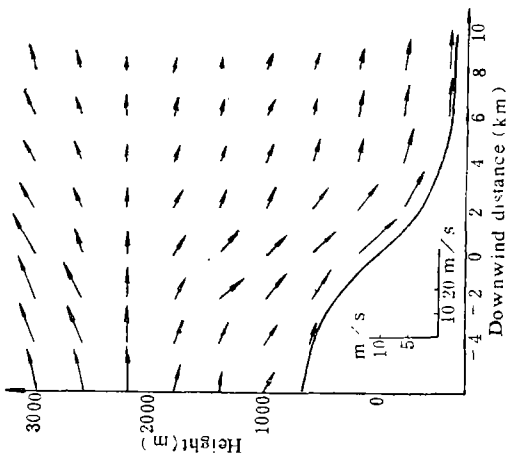


Fig. 1. Vertical cross section of the downslope flow field. The lower-left corner shows the velocity scale of the horizontal and the vertical components; solid line delineates the topographic profile; the parameters are taken as $h=3000\text{m}$, $a=500\text{m}$, $b=2000\text{m}$, $l_1=0.001\text{m}^{-1}$, $l_2=0.0005\text{m}^{-1}$, $\gamma=0.001\text{m}^{-1}$, $\alpha=0$.

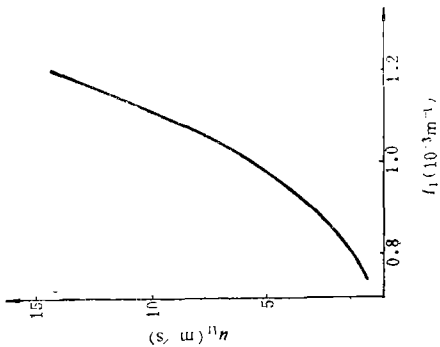


Fig. 2. Variation of the disturbed downslope wind speed (u_{1l}) with Scorer parameter (l_1). The lower layer mean wind speed $U_1=1.5\text{m/s}$. The parameters, but l_1 , are the same as in Fig. 1.

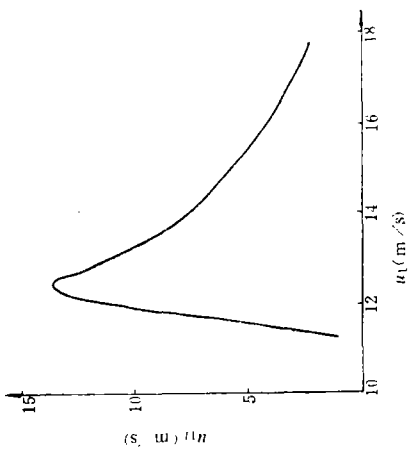


Fig. 3. Variation of the disturbed downslope wind (u_{1l}) with the lower layer mean wind speed (abscissa), $N_1=0.015\text{s}^{-1}$. The other parameters, but l_1 , are the same as in Fig. 1.

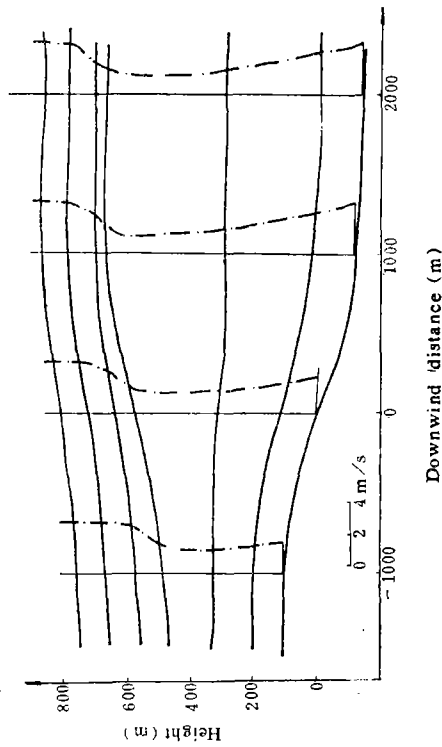


Fig. 4. Streamlines and horizontal wind profiles of drainage flow. The lower-left corner shows the horizontal wind speed scale. The parameters are taken as $h=3000\text{m}$, $a=1000\text{m}$, $b=500\text{m}$, $l_1=0.008\text{m}^{-1}$, $l_2=0.0025\text{m}^{-1}$, $\gamma=0.004\text{m}^{-1}$, $\alpha=2$, $U_1=2\text{m/s}$, $U_2=2.8\text{m/s}$.

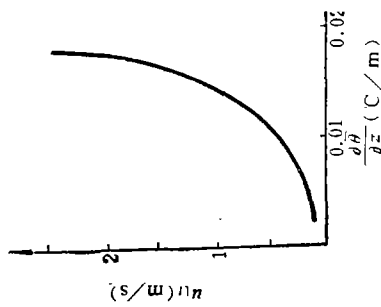


Fig. 5. Variation of the disturbed wind velocity of the drainage flow with stratification of the lower layer. The parameters, but l_1 , are the same as in Fig. 4.

reaches its maximum of about -8.8 m/s. And the downward momentum transport also reaches its maximum. Near the ground surface the disturbed horizontal wind speed at $x=4000$ m gets its maximum of about 20 m/s. Thus in the lower layer of the leeside the resulting velocity V can be 25–30 m/s, which is close to the value given by Klemp and Lilly (1975) in their analytical solution.

Since the streamlines diverge upward and downward at the height of about 2000 m over the leeside slope a weak wind region appears there. Then in the leeside the wind speed decreases with height. It indicates that the airflow at the lower levels in the leeside cannot gain the momentum from the higher levels by the turbulent gradient transport. The flow at the surface in the leeside can obtain the momentum from the higher levels upstream only by wave transport.

In the real atmosphere the wind speed at the lower end of the slope will decrease with the distance because of friction dissipation. Brinkmann (1974) analysed the distribution of the strong surface wind in the leeside of the Rocky Mountains. He concluded that wind maximum appears at the foot of the mountain, that is equivalent to $x=4-6$ km in Fig. 1.

Both of observation and theory reveal that the stable lower atmosphere is the necessary condition for leeside strong wind. Fig. 2 shows the variation of the disturbed surface wind, u_{1t} , with l_1 (that is, N_1 or $\partial\bar{\theta}_1/\partial z$) at a constant mean speed of $U_1=15$ m/s. It indicates that the disturbed wind speed increases with the stability.

It seems from Eq. (22) that the disturbed wind speed u_{1t} is proportional to U_1 . Since the mean wind speed U_1 in the lower layer, however, may induce the decrease of l_1 , the relation between u_{1t} and U_1 is not monotonous. Fig. 3 gives the relation between u_{1t} and U_1 at $N_1=1.5 \times 10^{-2} \text{ s}^{-1}$. It can be seen that the disturbed wind speed reaches its maximum at $U_1=12$ m/s. As the mean wind speed deviates from this value the disturbed wind speed always decreases.

2. Drainage Flow

The drainage flow occurs at clear night with weak wind when a strong surface inversion is formed by long wave radiative cooling. The wind is weak in the inversion while a strong wind region (low level jet) appears above the top of the inversion. It is assumed in the model that in the inversion the wind speed U_1 is uniform with the value of 2 m/s, the depth of inversion $h=300$ m, $N_1=0.016 \text{ s}^{-1}$, $l_1=0.008 \text{ m}^{-1}$. In the upper layer the wind is stronger and the stratification is less stable. For instance, $U_2=2.8$ m/s and $l_2=0.0025 \text{ m}^{-1}$. The parameters representing the density difference and wind shear between upper and lower layers are $\gamma=0.004 \text{ m}^{-1}$ and $\alpha=2$. The topographic parameters are taken as $a=100$ m and $b=500$ m.

Substituting these parameters into Eqs. (17) and (22), we have the disturbed streamlines ξ_{1t} and wind speed u_{1t} as shown in Fig. 4.

The streamlines in this figure also represent the distribution of the potential temperature. It can be seen that the stable layer over the upper end of the slope is shallow but strong; while the one over the lower end is deep but weak. This is in agreement with the observational analysis and numerical simulation (Sang, 1985).

In Fig. 4 the horizontal velocity is maximum near the ground surface. If the surface friction in the real atmosphere is considered, the wind maximum should appear between 10–30 m. The decrease of wind speed with height is caused by the effect of the return flow. As the mean wind speed is low and the return flow is strong, the region with negative horizontal velocity can be found in the real atmospheric observations. A wind speed jump occurs near the top of

the inversion to form a region of strong wind, that is the low level jet.

Taking the mean wind speed U_1 as a constant we can see from Eq. (22) that the strength of the drainage flow near the surface increases with l . Fig. 5 gives the variation of u_{11} at the surface with $\partial\theta/\partial z$. It shows that the speed of the drainage flow increases with the stability of the lower layer. This agrees with the results by Fleagle (1950), in which down-slope wind speed is proportional to the net radiation. It is reasonable that at a constant mean wind speed the stability in the lower layer is positively correlated with the net radiation.

It can be seen from Eq. (21) that the downward motion of the drainage flow is proportional to the height, a , and decreases with the width, b , of the terrain, that is, the descent speed increases with the slope of the terrain. This seems more reasonable than Fleagle's solution, in which the speed of the drainage flow is inversely proportional to the terrain slope.

Obtaining $k^* = 0.0044\text{m}^{-1}$, $v_1^* = 0.0067\text{m}^{-1}$ and $\mu^* = 0.0036\text{m}^{-1}$ from (18), substituting these parameters into (20), we have

$$\xi_{1h} = 14.6 \sin v_1^* (h+z) \cos k^* x,$$

as well as, $u_{1h} = -0.2 \cos v_1^* (h+z) \cos k^* x$

The value of u_{1h} at the surface $z = -h$ can reach 0.2m/s, which cannot be neglected. It indicates that the drainage flow is different from the strong downslope wind. In the drainage flow the higher wavenumber component has certain contribution to the disturbed wind speed. This short wave component presents periodic variation in the leeside downstream with wavelength of $2\pi/k^* = 1430\text{m}$. In some field observations surge exists in the drainage flow. Whether this phenomenon is related with the high wavenumber components is to be discussed in further studies.

REFERENCES

- Atkinson, B.W. (1981), *Meso-scale Atmospheric Circulations*, Academic Press, 495 pp.
- Brinkmann, W.A.R. (1974), Strong downslope winds at Boulder, Colorado, *Mon. Wea. Rev.*, **102**:592—602.
- Fleagle, R.E. (1950), A theory of air drainage, *J. Met.*, **17**:227—232.
- Klemp, J.B. and Lilly, D.K. (1975), The dynamics of wave-induced downslope winds, *J. Atmos. Sci.*, **32**:320—329.
- Sang Jianguo (1985), A theoretical study of airflow over an obstacle in neutral or slightly unstable atmosphere., *Arch. Met. Geoph. Biocl., Ser. A*, **34**:213—222.
- Sang Jianguo (1985), Numerical simulation of nighttime boundary layer over a slope terrain, *Acta Meteorologica Sinica*, **43**:458—468 (in Chinese).
- Scorer, R.S. (1978), *Environmental Aerodynamics*, Ellis Horwood Publisher, 488 pp.
- Smith, R.B. (1979), The influence of mountains on the atmosphere, *Advances in Geophysics*, **21**:87—230.